Gamma-ray spectroscopy in ^{110}Sn and ^{111}Sn

9th August 2004

M. Wolińska-Cichocka[1,2], J. Kownacki[1], E. Ruchowska[3], W.A. Płóciennik[3], W.Urban[2], B. Bekman[4], Ch. Droste[2], W. Gast[5], R. Lieder[5], W. Męczyński[6], M. Kisieliński[1,3], A. Kordyasz[1], M. Kowalczyk[1,2], P. Kowina[4], J. Iwanicki[1], T. Morek[2], J. Perkowski[7], J. Srebrny[2], A. Stolarz[1], J. Styczeń.[6]

[1] Heavy Ion Laboratory, Warsaw University, Pasteura 5A, 02-093 Warszawa, Poland,

[2]Institute of Experimental Physics, Warsaw University, Hoża 69, 00-681 Warszawa, Poland,

[3]The Andrzej Sołtan Institute for Nuclear Studies, Świerk, PL-05-400 Otwock-Świerk, Poland.

[4]Department of Physics, Silesia University, Katowice, Poland,

[5]Institut für Kernphysik, Forschungszentrum, Jülich, D-52425 Jülich, Germany,

[6] The H. Niewodniczański Institute of Nuclear Physics, 31-342 Kraków, Poland,

[7]Department of Physics, University of Łódź, ul. Pomorska 149/153, 90-286 Łódź, Poland.

Abstract

Excited states in ^{110}Sn and ^{111}Sn nuclei have been investigated using in-beam γ-ray spectroscopic methods. An ^{16}O beam with energy of 60-80 MeV was used to bombard a ^{98}Mo target. On the basis of the relative excitation functions, γ-ray angular distributions, $\gamma-\gamma$ and $\gamma-time$ coincidences, γ-ray multiplicity and total energy data the level schemes of ^{110}Sn and ^{111}Sn have been re-investigated and extended up to $E_{exc} \sim 11.5$ MeV and I=24$\hbar$, and $E_{exc} \sim 11.1$ MeV and I=(51/2)$\hbar$, respectively. An extension of the intruder, g.s. and negative parity bands in ^{110}Sn in low-spin region as well as 5 new band-like structures are proposed. In the ^{111}Sn nucleus an intruder band based on $23/2^-$ state has been reinvestigated and the extension of the g.s. band and second negative parity band is given. An evidence for neutron-core coupling in ^{111}Sn is found. The structure and systematics of the excited states in light Sn isotopes is discussed.

PACS. 27.60+j; 25.70.Gh; 23.20.Lv; 21.60.Cs; 21.10.Re $90 \leq A \leq 149$

Keywords: Nuclear Reactions $^{98}Mo(^{16}O, xnyp)$, E = 60, 70, 75 and 80 MeV; measured E_γ, I_γ, $I_{\gamma\gamma}(\Theta)$, $\gamma\gamma$-coin., ^{110}Sn, ^{111}Sn deduced levels, J, π. Enriched target, array of Compton-supressed Ge detectors, shell model, crank shell model and total routhian surface calculations.

1 Introduction.

The neutron shell N=50-82 contains the positive parity $s_{1/2}$, $d_{3/2}$, $d_{5/2}$ and $g_{7/2}$, and the unique parity high-j $h_{11/2}$ orbitals. At the beginning of the shell, the ground state of nuclei is formed by the $d_{5/2}$ orbital and in ^{111}Sn it shifts to the $g_{7/2}$ configuration. Hence, the low part of the ^{110}Sn level scheme is expected to be dominated by the neutron $d_{5/2}$ and $g_{7/2}$ excitations. Spherical states in this part of the level scheme are interpreted as pure neutron configurations, while at higher energies the deformed "p-h intruding" excitations across the proton closed Z=50 shell become important. Excitations of this type are expected to deform nuclei and to generate rotational bands.

The low spin states in ^{110}Sn have previously been investigated in the ^{110}Sb decay [1] as well as in a number of reaction studies [2, 3, 4, 5], where the existence of the 5.6 ns, 6^+ isomer decaying through the 280, 985 and 1212 keV transitions has been well proven. The odd-A tin isotopes have been of interest because of intruder bands observed in ^{111}Sn and ^{113}Sb [6, 7]. The excited states of the ^{111}Sn nucleus have been previously investigated in the β-decay of ^{111}Sb [8] as well as in in-beam experiments including both single nucleon transfer [9] and heavy ion reactions [6].

There are, however, still several reasons for the investigation of light Sn nuclei:

1) Rotational bands proposed to be built on proton 2p-2h excitations have been observed in the $^{116-118}$Sn even-mass nuclei down to the 0^+ band heads [3], whereas in ^{110}Sn and ^{112}Sn no intruder band members below spin $10\hbar$ have been observed [4, 5]. The odd-mass Sn nuclei, like ^{111}Sn, are believed to have a rotational band constructed of the valence neutron coupled to the 2p-2h intruder states in even-Sn nuclei. It is important to show the presence of enhanced intra-band B(E2) values and hindered or much reduced inter-band decays [10] in order to reasaon shape coexsistence in these nuclei.

2) The regular level energy systematics of excited states in even Sn nuclei appear to break in the case of ^{110}Sn.

3) Several states are "missing", e.g. the second 10^+, 3^-, 5^- states, and several low spin members of the negative parity and intruder bands are not known.

4) Middle and high spin states in ^{111}Sn could yield additional information on side bands, particle-core coupling and on the existence of high-spin isomeric states.

In this paper the main interest is focused on the structure of ^{110}Sn and ^{111}Sn isotopes.

The spectroscopic studies have been performed with the aim to gather more information on the intruder bands and their systematic behaviour as well as to resolve some ambiguities concerning level schemes of these nuclei.

Preliminary results of these study have been published in refs. [11, 12].

2 Experimental procedure and results.

The experimental information presented in this paper results from measurements performed at the Heavy Ion Laboratory cyclotron of the Warsaw University. Enriched ^{98}Mo targets with a thickness of $3 - 5.6\ mg/cm^2$ were bombarded with ^{16}O beam at four energies: 60, 70, 75 and 80 MeV. The beam was formed into bunches consisting of many short ($\sim$ 70 ns) cyclotron beam pulses. The duration of the bunches was adjustable and changed from 1.5 to 3 ms (repeated every 6 ms) in different runs. The beam energies were determined from the radio-frequency of

the cyclotron and using TOF techniques, which implied the accuracy of ~ 0.5 MeV.
The relative yield for the reaction channels leading to doubly even final nuclei was deduced from the γ-ray yields for the $2^+ \rightarrow 0^+$ transitions on the assumption that the side-feeding to the ground state could be neglected. The relative yield for the channels leading to odd-A or odd-odd final nuclei was assumed to correspond to the sum intensities of all known transitions leading to the ground state. The compound nucleus ^{114}Sn* favored the evaporation of neutrons, hence 3n and 4n reaction channels were expected to be the strongest reaction channels. However, yields of the p2n, p3n and especially α evaporation channels were also relatively strong at the 80 MeV bombarding energy (see Table.1). The production of ^{110}Cd nuclei (α evaporation channel) was additionally increased due to radioactive decay of ^{110}In (4.9 h and 69.1 m).
The OSIRIS-II array consisting of 10 Compton-suppressed HPGe detectors combined with a 48-elements BGO sum-energy and multiplicity filter was used in the measurements . The HPGe detectors were located behind the filter, and the BGO crystals served as collimators for them. The Ge detectors were placed in two rings; in the first one at angles $\Theta = \pm 38^o, 87^o, 90^o, \pm 142^o$ and in the second one at $\Theta = 25^o, 63^o, 117^o, 155^o$ with respect to the beam direction . Relative excitation functions, γ-ray angular distributions, linear polarization data (ref. [11]), and prompt and delayed (in millisecond and nanosecond regions) γ-ray singles and $\gamma\gamma$ coincidence spectra have been measured.

Table 1: *Relative yields for channels observed in the ^{16}O (80 MeV) + ^{98}Mo reaction. Below each symbol of the final nucleus the pertinent reaction channel is followed by the respective relative yield. Those yields are given as a percentage of the total reaction yield evaluated from intensities of γ-lines leading to the ground state of the final nucleus in each reaction channel.*

N\Z	**60**	**61**	**62**	**63**	**64**
50	^{110}Sn *4n* **18.4(5)**	^{111}Sn *3n* **17.8(4)**	^{112}Sn *2n* **2.9(9)**	^{113}Sn *n* **<0.2**	^{114}Sn *CN*
49	^{109}In *p4n* **1.2(9)**	^{110}In *p3n* **5.2(20)**	^{111}In *p2n* **8.1(5)**	^{112}In *np* **<0.2**	^{113}In *p*
48	^{108}Cd *2p4n* **6.2(5)**	^{109}Cd *2p3n* **0.7(6)**	^{110}Cd *2p2n* **33.0(3)**	^{111}Cd *2pn* **4.2(5)**	^{112}Cd *2p*
47	^{107}Ag *3p4n* **<0.2**	^{108}Ag *3p3n* **0.8(7)**	^{109}Ag *3p2n* **<0.2**	^{110}Ag *3pn* **0.9(8)**	^{111}Ag *3p*

The isotopic assignment of γ-rays following the $^{98}Mo(^{16}O, xnyp)$ reaction was supported by the behavior of their yields as function of the bombarding energy. Examples of relative excitation functions measured for the most prominent γ-rays assigned to the 4n and 3n reaction channels are shown in Figs. 1 and 2. The relative excitation functions for the γ-rays depopulating non-yrast levels exhibit usually patterns which differs from that of the yrast states. Quite pronounced differences occur for low spin levels, when compared to the yrast states with

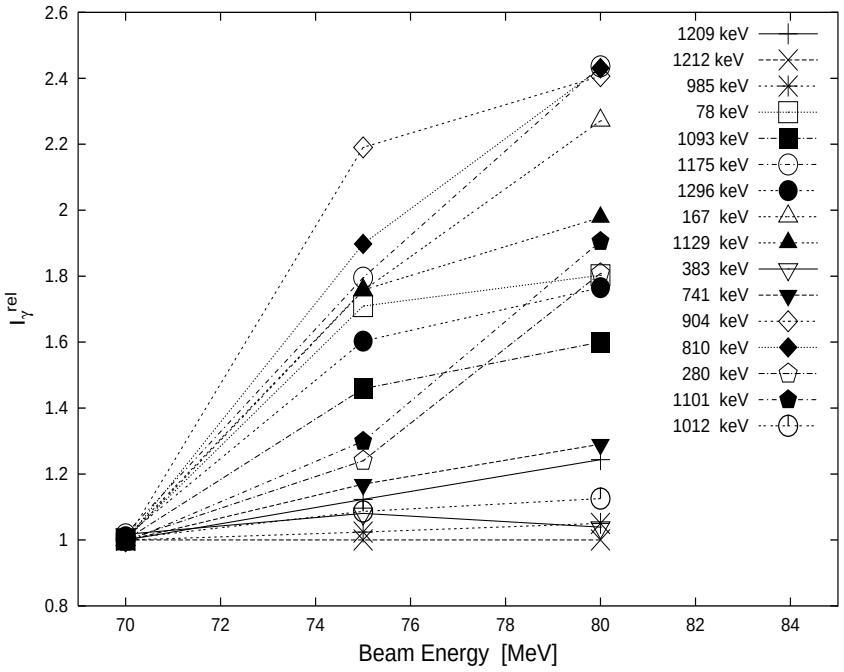

Figure 1: Relative excitation functions determined for selected γ-rays from the $^{98}Mo(^{16}O, 4n\gamma)^{110}Sn$ reaction.

corresponding spin. The 808, 741, 810 and 904 keV γ-rays from the cascade feeding to the 10^+, 5227 keV yrast state in ^{110}Sn have clearly the steepest relative excitation functions, suggesting relatively high spins of their initial levels. Similarly, the 768, 803, 869, 942 and 1091 keV γ-rays in ^{111}Sn (Fig. 2) show a steep behavior indicating that they are emitted from states with rather high spins.

A total of $\sim 10^8$ events were recorded in the $\gamma\gamma$ coincidence measurements. The data were sorted off-line into several $\gamma\gamma$ matrices with various time conditions (prompt and off-beam with several time windows) and various combinations of detector angles. Specific conditions were put on multiplicity and total energy in order to enhance the desired reaction channel. The analysis of $\gamma\gamma$ matrices and construction of the level schemes was performed using the RadWare software package [13].
Examples of the coincidence spectra illustrating the main features of the level schemes are shown in Figs. 3 and 4.

The conventional angular distribution measurements were performed at six different angles with respect to the beam axis. The data were normalized to transitions with isotropic angular distributions from the radioactivity spectrum and corrected for the efficiency of individual detectors. Subsequently, the resulting intensities were normalized to those observed at 90^o. The $\gamma\gamma$ matrices sorted for different combinations of detector angles were used to investigate angular correlations between the emitted γ-rays. The multipolarities of new γ-transitions were also derived from R_{DCO} ratios defined as:

$$R_{DCO} = \frac{I_\gamma(E_\gamma; 38^o + 25^o)}{I_\gamma(E_\gamma; 90^o + 87^o)} \quad (1)$$

In order to determine the ratios the data were sorted into $E_\gamma - E_\gamma$ matrices with the following angle combinations: (i) $(38^o + 25^o)$ vs. all angles and (ii) $(90^o + 87^o)$ vs. all angles, where

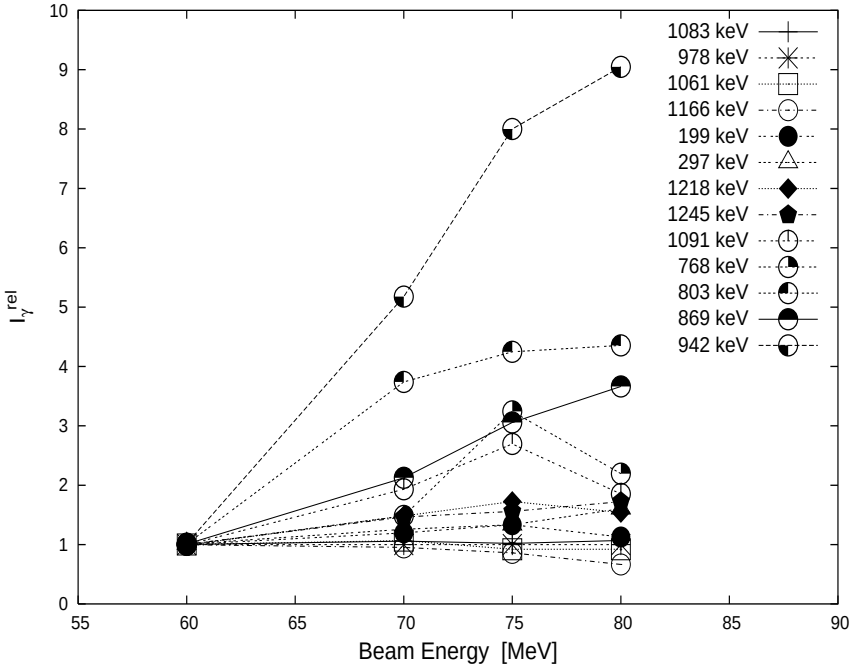

Figure 2: Examples of relative excitation functions for selected γ-rays from the $^{98}Mo(^{16}O, 3n\gamma)^{111}Sn$ reaction.

first the x-axis and then the y-axis is given. By setting identical gates on the desired γ-rays in both matrices, coincidence spectra were created from which the intensity ratio $R(E_\gamma)$ could be extracted. To make the spin-parity assignments, it was assumed that the observed transitions were of E1, M1 or E2 type. The obtained ratios have values around 0.6 and 1.0 (Fig. 5). The first value corresponds to dipole $I \rightarrow I-1 (I-1 \rightarrow I)$ transitions, while the second to stretched quadrupole $I \rightarrow I-2 (I-2 \rightarrow I)$ and non-stretched ($\Delta I = 0$) dipole transitions. In many cases, the same state is reached via various decay paths, which helps to resolve ambiguities.

3 The level schemes.

3.1 The nucleus ^{110}Sn.

The level scheme based on the data obtained in the ^{98}Mo$(^{16}O, 4n\gamma)^{110}Sn$ reaction is shown in Fig. 6 where eight band-like structures are presented. The γ-rays assigned to ^{110}Sn together with their relative intensities, angular distribution coefficients and DCO ratios as well as spins and parities proposed for the initial and final states are listed in Table 2. Part of the level scheme up to the 6^+, $\sim$ 5.6 ns, 2477 keV isomer (band 5), and band 3 up to the 20^+, $\sim$ 9.5 MeV state were already known from earlier experiments [2, 3, 4, 5].

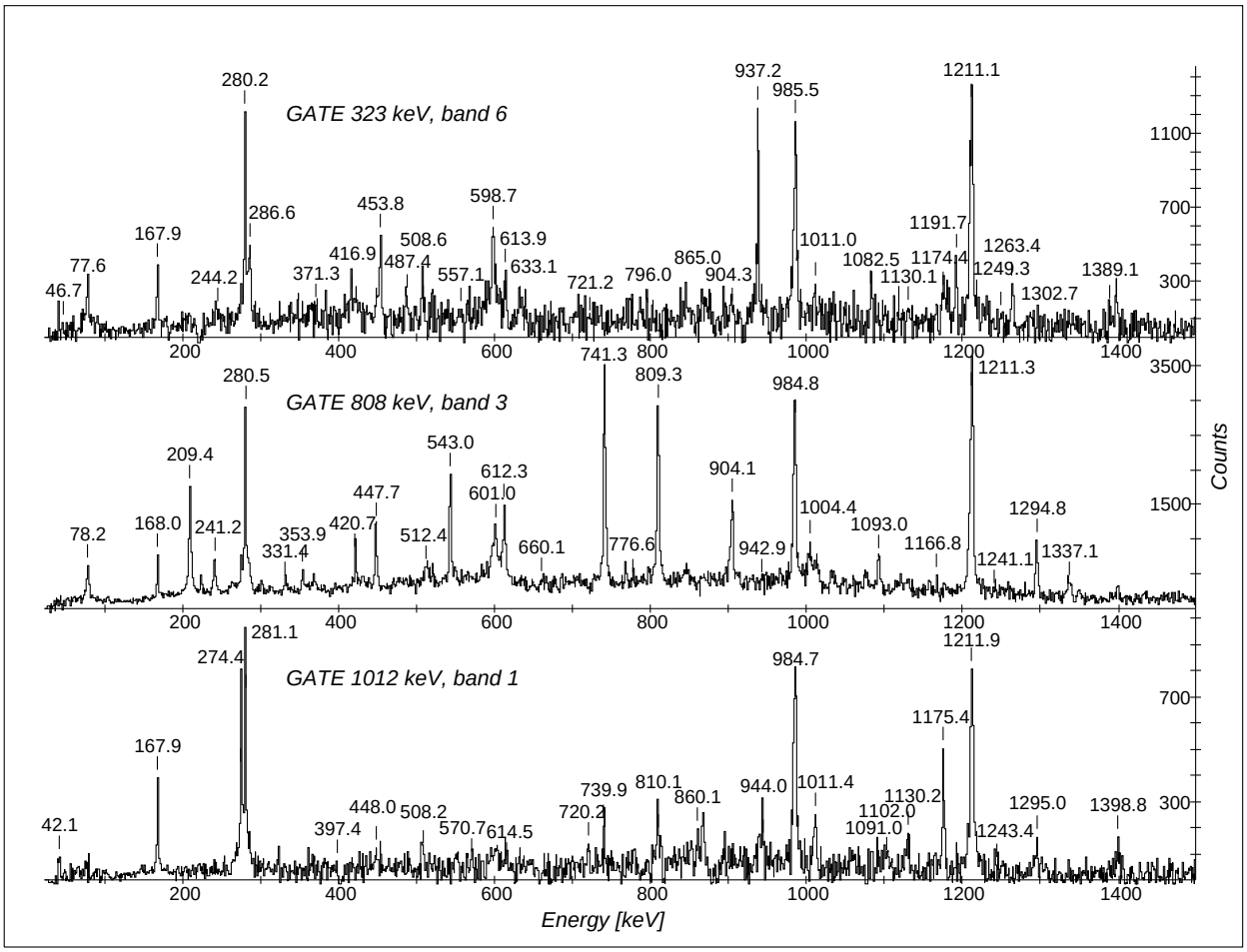

Figure 3: Examples of coincidence spectra obtained in the $^{98}Mo(^{16}O, 4n\gamma)$ reaction at a bombarding energy of 80 MeV. Representative gates for the ground state band (5), intruder band (3), and negative parity band (1) are selected. The 937 keV γ-ray (which might be ascribed to the ^{110}Cd and ^{108}Ag nuclei) is observed in the 323 keV gate due to the presence of 2p2n (^{110}Cd), α2n (^{108}Cd) and αpn (^{108}Ag) reaction channels.

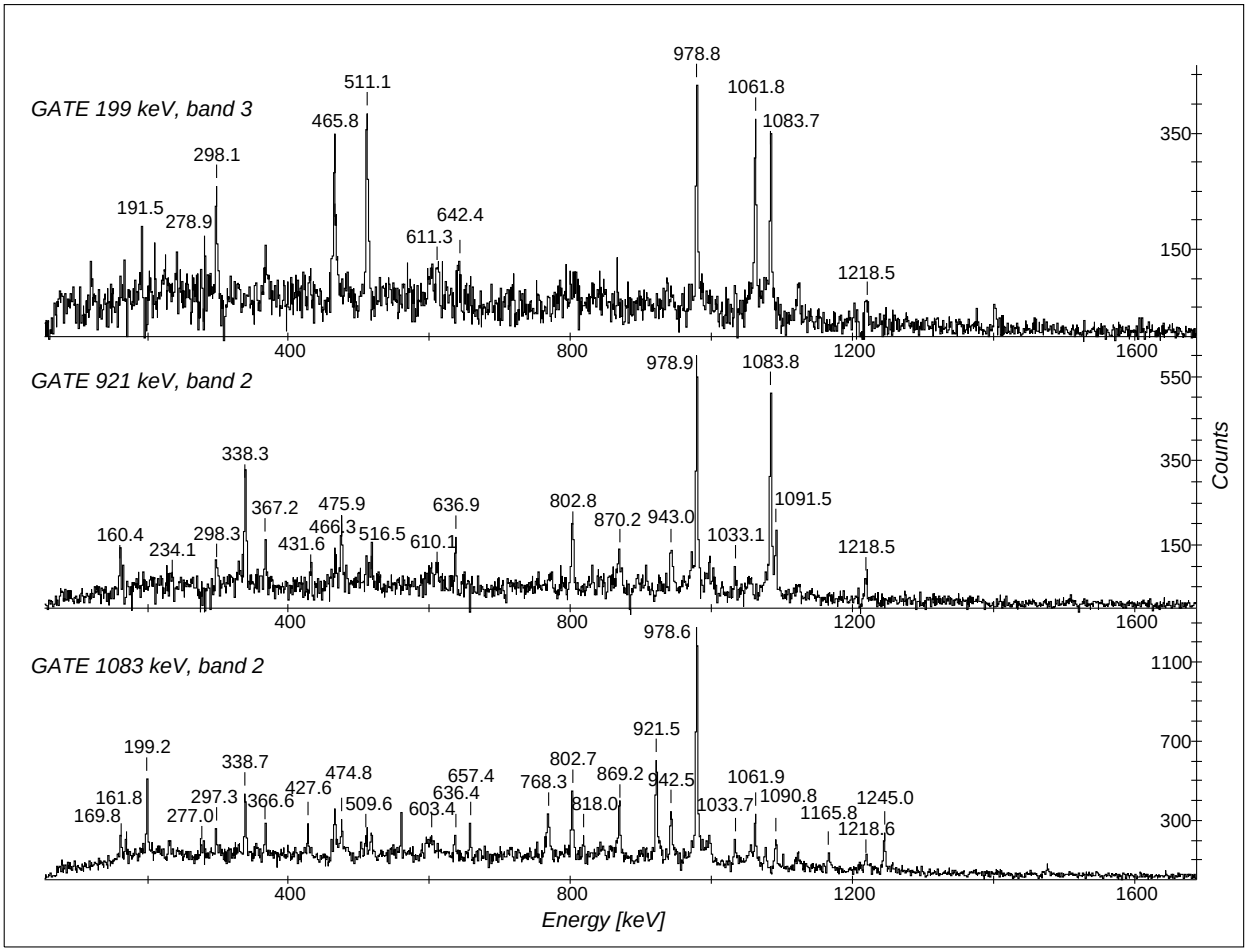

Figure 4: Sample of the background-corrected, $\gamma\gamma$ coincidence spectra for bands in ^{111}Sn populated in the $^{98}Mo(^{16}O, 3n\gamma)$ reaction at 80 MeV

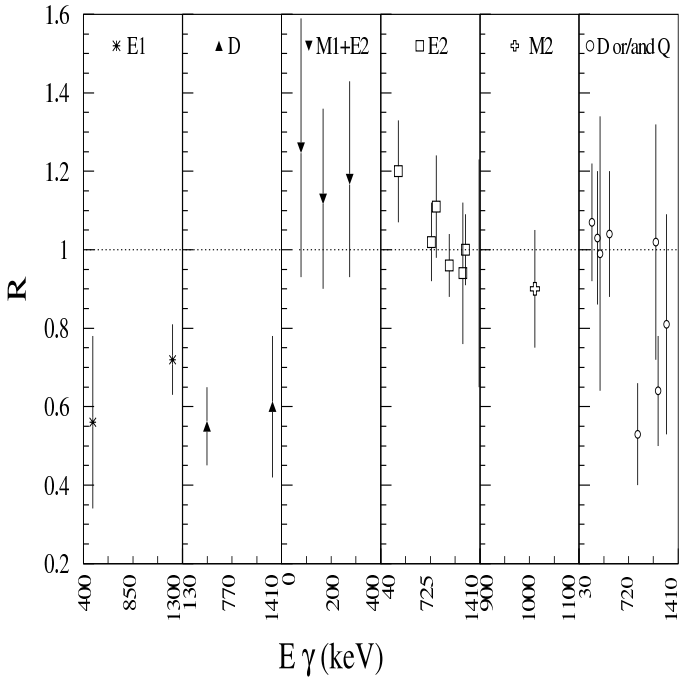

Figure 5: DCO ratios determined for selected γ-rays from the $^{98}Mo(^{16}O, xn)$ reaction.

Table 2: *Gamma-ray transitions assigned to* ^{110}Sn*. Excitation energies of the initial level,* γ*-ray energies, relative* γ*-ray intensities, angular correlations ratios* R_{DCO}*, angular distribution coefficients* $W(\theta)$*, and the proposed spin and parity assignments are given.*

E_i (keV)	E_γ (keV)	I_γ (relative)	R_{DCO}	$W(\theta)$		$J_i^\pi \rightarrow J_f^\pi$ ($\hbar$)
				A_2/A_0	A_4/A_0	
1212	1211.8(0.4)	100(8)	1.00(09)	0.20(7)	-0.07(4)	$2^+ \rightarrow 0^+$
2058	846.0(0.4)	4.6(1)	—	—	—	$(0,2) \rightarrow 2^+$
2197	984.6(0.4)	83(3)	0.96(08)	0.29(7)	-0.01(1)	$4^+ \rightarrow 2^+$
2455	1242.5(0.8)	1.7(7)	—	—	—	$(2,4) \rightarrow 2^+$
2458	261.5(0.2)	1.9(2)	—	—	—	$3^- \rightarrow 4^+$
2458	1246.4(0.2)	4.8(6)	—	-0.16(5)	0.01(2)	$3^- \rightarrow 2^+$
2477	280.2(0.3)	57(2)	1.20(13)	0.11(1)	-0.14(9)	$6^+ \rightarrow 4^+$
2591	1379.0(0.5)	2.3(7)	—	—	—	$(0^+) \rightarrow 2^+$
2742	1530.1(0.8)	1.7(5)	—	—	—	$(0,1,2,3) \rightarrow 2^+$
2752	275.3(0.4)	10.3(3)	1.18(25)	0.35(9)	-0.01(2)	$6^+ \rightarrow 6^+$
2800	323.1(0.1)	2.8(2)	—	—	—	$(6^+) \rightarrow 6^+$
2800	603.4(0.1)	5.9(5)	—	—	—	$(6^+) \rightarrow 4^+$
2821	624.0(0.9)	0.8(4)	—	—	—	$(2,3,4,5) \rightarrow 4^+$
2821	1609.8(0.6)	2.3(6)	—	J=3: 0.10(10) J=4: 0.06(6)	J=3: 0.01(1) J=4: $-0.15(15)$	$(3,4) \rightarrow 2+$
2847	256.0(0.6)	0.2(1)	—	—	—	$(2^+) \rightarrow (0^+)$
2963	163.9(0.1)	0.9(1)	—	—	—	$5^- \rightarrow (6^+)$
2963	486.0(0.1)	1.3(1)	0.56(22)	-0.44(14)	0.01(2)	$5^- \rightarrow 6^+$

2963	505.8(0.2)	1.1(1)	—	—	—	$5^- \rightarrow 3^-$
3210	1013.8(0.3)	4.0(6)	—	J=3: 0.15(20) J=5: 0.15(20)	J=3: 0.003(7) J=5: 0.01(2)	(3,5)→4+
3215	367.7(0.8)	0.15(4)	—	—	—	$(4^+) \rightarrow (2^+)$
3249	285.4(0.7)	2.0(3)	1.03(17)	-0.13(19)	0.04(7)	$(4) \rightarrow 5^-$
3320	843.5(0.1)	4.7(4)	0.53(13)	—	—	$4^+ \rightarrow 6^+$
3320	864.0(0.5)	1.2(2)	—	—	—	$4^+ \rightarrow$(2,4)
3334	857.9(0.4)	1.2(3)	—	—	—	$(6^+) \rightarrow 6^+$
3354	602.1(0.3)	1.5(1)	—	—	—	$(5^-) \rightarrow 6^+$
3354	896.2(0.3)	2.3(3)	—	—	—	$(5^-) \rightarrow 3^-$
3416	453.4(0.1)	1.4(3)	1.04(16)	0.36(20)	0.06(9)	$6^- \rightarrow 5^-$
3416	938.3(0.3)	1.8(3)	—	—	—	$6^- \rightarrow 6^+$
3416	1219.3(0.2)	6.0(5)	—	—	—	$6^- \rightarrow 4^+$
3686	270.8(0.2)	1.8(1)	—	—	—	$7^- \rightarrow 6-$
3686	332.0(0.1)	0.2(1)	—	—	—	$7^- \rightarrow (5^-)$
3686	437.2(0.3)	0.7(1)	—	—	—	$7^- \rightarrow (4)$
3686	933.9(0.2)	1.7(1)	—	-0.22(9)	0.01(1)	$7^- \rightarrow 6^+$
3686	1208.8(0.5)	31(1)	0.72(09)	-0.29(9)	0.01(1)	$7^- \rightarrow 6^+$
3686	1228.1(0.7)	0.8(2)	—	—	—	$7^- \rightarrow 3^-$
3764	78.3(0.1)	13.8(5)	1.26(33)	0.07(5)	0.06(3)	$8^- \rightarrow 7^-$
3764	1012.3(0.1)	5.2(3)	0.90(15)	0.30(12)	-0.06(7)	$8^- \rightarrow 6^+$
3764	1287.5(0.5)	0.9(1)	—	—	—	$8^- \rightarrow 6^+$
3812	1335.0(0.1)	2.3(2)	—	0.36(15)	-0.03(4)	$(8^+) \rightarrow 6^+$
3813	597.6(0.1)	3.5(4)	—	—	—	$(6^+) \rightarrow (4^+)$
3931	167.5(0.1)	12.7(4)	1.13(23)	—	—	$9^- \rightarrow 8^-$
3991	1191.1(0.3)	1.9(3)	—	—	—	$(8^+) \rightarrow (6^+)$
4002	1249.9(0.2)	2.1(2)	0.81(28)	0.47(37)	0.13(10)	$(7^+) \rightarrow 6^+$
4137	816.7(0.1)	4.4(3)	—	—	—	$(6^+) \rightarrow 4^+$
4279	945.4(0.5)	0.8(2)	—	—	—	$(8^+) \rightarrow (6^+)$
4314	311.7(0.2)	1.1(1)	—	0.25(21)	0.02(2)	$(8^+) \rightarrow (7^+)$
4314	382.7(0.4)	0.5(1)	—	—	—	$(8^+) \rightarrow 9^-$
4425	611.7(0.1)	2.6(3)	—	—	—	$8^+ \rightarrow (6^+)$
4779	848.5(0.9)	0.2(1)	—	—	—	$9^- \rightarrow 9^-$
4779	967.4(0.4)	0.3(1)	—	—	—	$9^- \rightarrow (8^+)$
4779	1092.9(0.1)	3.6(3)	—	0.24(11)	-0.09(5)	$9^- \rightarrow 7^-$
4880	743.2(0.1)	3.2(3)	—	—	—	$(8^+) \rightarrow (6^+)$
4893	1129.5(0.1)	6.1(3)	0.64(14)	0.26(11)	-0.08(7)	$10^- \rightarrow 8^-$
5016	1203.7(0.2)	2.1(2)	—	—	—	$(10^+) \rightarrow (8^+)$
5106	1175.3(0.5)	8.9(3)	0.94(18)	0.33(8)	-0.05(2)	$(11^-) \rightarrow 9^-$
5218	1227.4(0.4)	0.7(1)	—	—	—	$(10^+) \rightarrow (8^+)$
5227	211.0(0.2)	0.8(0)	1.07(15)	-0.15(1)	-0.20(22)	$10^+ \rightarrow (10^+)$
5227	331.6(0.3)	0.5(0)	—	—	—	$10^+ \rightarrow 10^-$
5227	447.7(0.8)	3.4(1)	0.55(10)	-0.35(16)	0.001(3)	$10^+ \rightarrow 9^-$
5227	801.8(0.1)	2.8(1)	—	—	—	$10^+ \rightarrow (8^+)$
5227	912.8(0.7)	0.3(0)	—	—	—	$10^+ \rightarrow (8^+)$
5227	1295.6(0.1)	1.9(1)	0.60(18)	0.40(36)	0.16(18)	$10^+ \rightarrow 9^-$

5329	1397.6(0.1)	2.7(1)	0.94(29)	0.19(8)	-0.11(6)	$(11^-) \rightarrow 9^-$
5730	849.7(0.2)	1.4(2)	—	—	—	$(10^+) \rightarrow (8^+)$
5817	487.4(0.5)	$\leq$0.1	—	—	—	$(8) \rightarrow (11^-)$
5936	119.0(0.1)	0.3(2)	—	—	—	$(9) \rightarrow$
5936	604.5(0.6)	$\leq$0.1	—	—	—	$(9) \rightarrow (11^-)$
6035	808.2(0.1)	9.8(6)	1.11(13)	0.43(10)	-0.01(1)	$(12^+) \rightarrow 10^+$
6035	816.9(0.4)	0.8(1)	—	—	—	$(12^+) \rightarrow (10^+)$
6035	1019.1(0.9)	0.4(1)	—	—	—	$(12^+) \rightarrow (10^+)$
6064	127.4 (0.1)	0.3(1)	—	—	—	$(10) \rightarrow (9)$
6205	140.2(0.2)	0.2(0)	—	—	—	$(11) \rightarrow (10)$
6205	874.6(0.4)	0.8(1)	—	—	—	$(11) \rightarrow (11^-)$
6205	978.2(0.1)	1.3(4)	—	—	—	$(11) \rightarrow 10^+$
6205	1100.7(0.1)	2.5(1)	0.90(15)	—	—	$(11) \rightarrow (11^-)$
6353	147.7(0.3)	0.3(0)	—	—	—	$(12) \rightarrow (11)$
6353	318.0(8.0)	0.1(1)	—	—	—	$(12) \rightarrow (12^+)$
6370	1041.0(1.0)	0.3(1)	—	—	—	$(12) \rightarrow (11^-)$
6544	1215.3(0.1)	1.4(2)	—	—	—	$(13) \rightarrow (11^-)$
6597	867.8(0.2)	1.3(1)	—	—	—	$(12^+) \rightarrow (10^+)$
6613	259.6(0.5)	0.3(0)	—	—	—	$(13) \rightarrow (12)$
6776	740.9(0.1)	9.7(4)	1.02(10)	0.29(9)	-0.06(7)	$(14^+) \rightarrow (12^+)$
6974	361.2(1.0)	0.1(1)	—	—	—	$(14) \rightarrow (13)$
7540	942.8(0.2)	1.6(1)	—	—	—	$(14^+) \rightarrow (12^+)$
7586	809.9(0.1)	10.4(5)	1.11(13)	0.43(11)	-0.01(1)	$(16^+) \rightarrow (14^+)$
8490	903.9(0.1)	4.2(0)	—	0.17(17)	-0.10(16)	$(18^+) \rightarrow (16^+)$
9493	1003.3(0.1)	2.7(2)	—	—	—	$(20^+) \rightarrow (18^+)$
10501	1007.6(0.2)	1.3(1)	—	—	—	$(22^+) \rightarrow (20^+)$
11515	1014.5(0.2)	1.3(1)	—	—	—	$(24^+) \rightarrow (22^+)$

3.1.1 Band 5. The 1212, 2197, 2477 keV levels

The γ-ray cascades displayed in Fig. 6 proceed through the positive and negative parity states and feed mainly the lowest 2^+, 4^+ and 6^+ states with energies of 1212, 2197 and 2477 keV, respectively. These states are deexcited by the three most intense γ-rays observed in the $^{98}Mo(^{16}O, 4n\gamma)^{110}$Sn reaction which have energies 1212, 985 and 280 keV and constitute a stretched E2 yrast cascade. This assignment is strongly confirmed in the present work by the relative excitation functions, coincidence results, angular distributions, lifetime estimates and DCO ratios.

3.1.2 Band 1

Existence of a low-lying 3^- state at an energy of 2458 keV was suggested in a $^{112}Sn(p,t)$ reaction study [14]. In the present work the 3^- state is confirmed at an energy of 2458 keV, as a coincidence was observed between new 1246 keV γ-ray and the 1212 keV, $2^+ \rightarrow 0^+$ transition, and with the 896 keV transition dexciting the 3354 keV, as suggested (5^-) level. A candidate for the another 5^- state is also the 2963 keV level connected with the 6^+, 2477 keV state by the

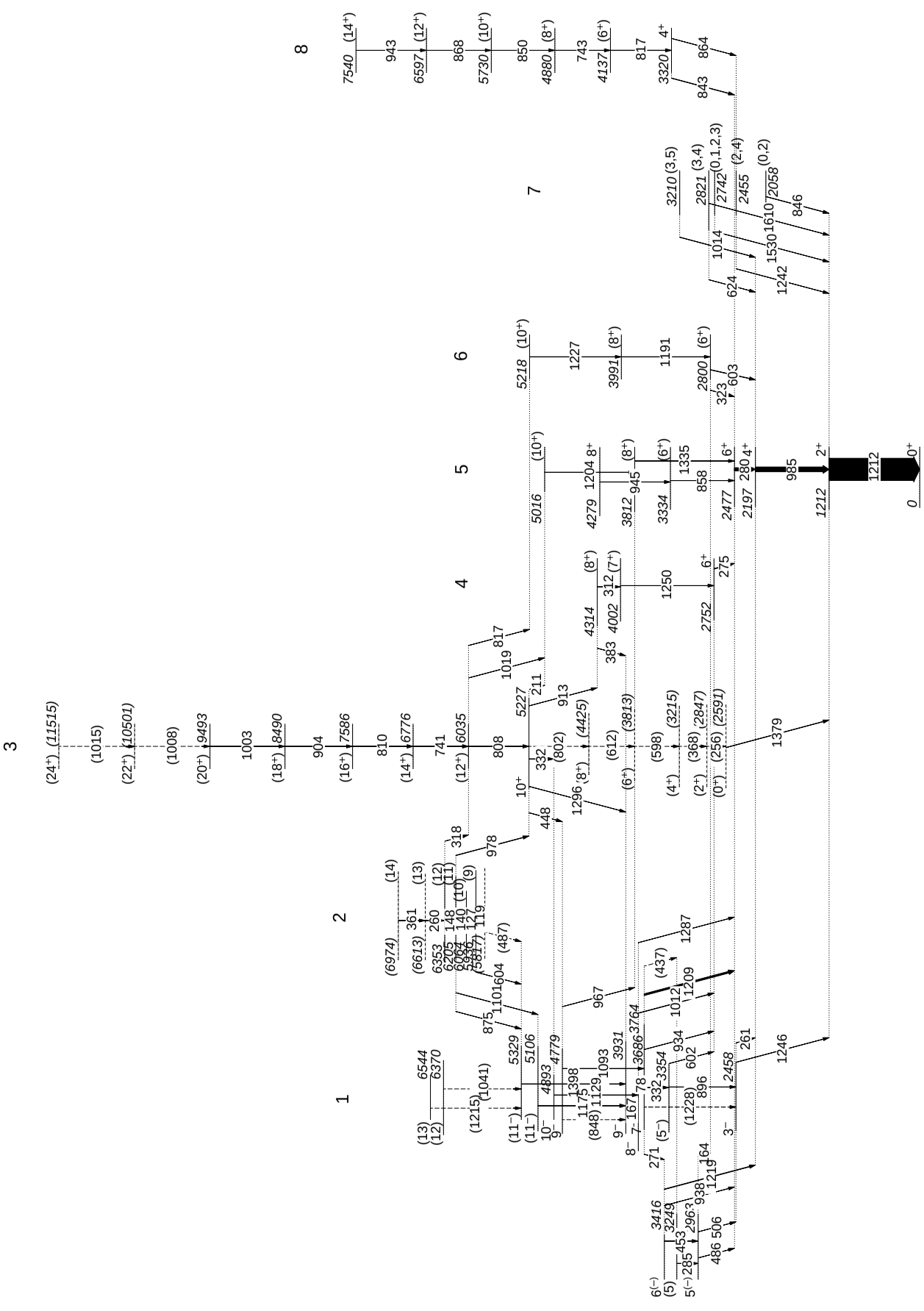

Figure 6: The level scheme of ^{110}Sn, as observed in the $^{98}Mo(^{16}O, 4n\gamma)$ reaction.

486 keV γ-ray showing a strong negative anisotropy of A_2/A_0=-0.44 and A_4/A_0=0.01, consistent with expectations for a $5^- \rightarrow 6^+$, E1 transition. The 453 keV γ-ray observed in coincidence with the 486 keV transition deexcites a new level introduced at 3416 keV. The 453 keV γ-ray is probably of dipole, M1 character, with a significant admixture of the E2 component, suggesting a $6^{(-)}$ spin-parity assignment for the 3416 keV level. Observation of γ-transitions linking the 3416 keV level with the 3^-, 2458 keV and 7^-, 3686 keV states additionally support both the placement and spin-parity assignments of the 2963 keV and 3416 keV levels.

The 3249 keV level.

The 3249 keV level was introduced in the (p,t) reaction study [14] with an $l = 4$ assignment, however no γ-rays feeding or deexciting this level were known. In the present study the energy of 3249 keV is determined for this level by observing a new 285 keV transition connecting this state with the $5^{(-)}$, 2963 keV level. Because of its negative anisotropy this transition can be classified as a mixed dipole-quadrupole transition, suggesting a spin assignment I=4 or 5 for the 3249 keV level. Observation of a weak coincidence of the 285 keV γ-ray with the 437 keV one deexciting the 7^-, 3686 keV state is in favour of I=5 assignment.

The 7^-, 3686 keV, 8^-, 3764 keV and 9^-, 3931 keV levels.

These levels are confirmed in the present study due to the observation of the 934 keV and 1209 keV transitions of dipole, most probable E1 character, deexciting the 3686 keV state. Besides, four new γ-rays of energies 271, 332, 437 and 1228 keV deexciting the 3686 keV state were also observed.

The 4779, 4893, 5106 and 5329 keV levels.

The 4779 keV level deexcites through the 1093 keV transition of quadrupole character, according to angular distribution results, most probably E2 character feeding the 7^-, 3686 keV level. This suggests a 9^- spin-parity assignment for this level. The observation of a 448 keV γ-ray linking this level with the 10^+, 5227 keV level and of weak 848 and 967 keV transitions depopulating this level gives further support for the 9^- assignment. The 4893, 5106 and 5329 keV levels are deexcited via the 1129, 1175 and 1398 keV γ-rays, respectively. The 6370 keV and 6544 keV levels introduced here are based on the coincidence relations of 1041 and 1215 keV γ-rays, and are candidates for the $12^{(-)}$ and $13^{(-)}$ states. However, no definite conclusions concerning the parity assignments for these two levels have been obtained.

3.1.3 Band 2.

A new sequence of levels showing a $\Delta I = 1$ structure is observed. This band decays via weak γ-rays to band 1 and band 3. Tentative spin assignments are based on the dipole character of the 604 and 1101 keV transitions. Further investigations are needed.

3.1.4 Band 3.

An intruder band consisting of a cascade of the 808, 741, 810, 904 and 1003 keV γ-rays as established in [2, 3] is confirmed in the present work (see Fig. 3, spectrum gated on the 808 keV γ-ray). An extension of this band towards higher spins (22^+ and 24^+) is proposed, based on the coincidence data and intensity relations. Also low spin members of the intruder band have been established, based on the observation of a cascade of 1379, 256, 368, 598, 612 and 802 keV transitions linking the 10^+, 5227 keV level with the 1212 keV state. Fig. 7 shows examples of the $\gamma\gamma$ coincidence spectra for the low spin part of the intruder band. In addition

to this cascade, other transitions linking band 3 with levels belonging to bands 1, 4, 5 and 6 have been observed. In particular, the decay of the 10^+, 5227 keV level is well fragmented. Also the (12^+) state at 6035 keV decays via 808, 817 and 1019 keV transitions, most probably of E2 character, feeding three 10^+ states.
A comparison of preliminary experimental ratios

$$K_{exp} = \frac{B(E2)_{intraband}}{B(E2)_{interband}} \tag{2}$$

for the intruder bands in light Sn nuclei obtained in the present work has been published elswhere, ref. [12]. An extended version of this data, given in Table 3, shows rather strong intra-band B(E2) values as compared to the hindered inter-band decays. The upper limits for the B(E2), γ-ray branching ratios for the non forbidden transitions of 760, 1626, 1955 and 2014 keV (not placed in the level scheme) are also given.

An indication for the existence of a high spin isomeric state feeding the (16^+), 7586 keV level of the intruder band has been found in the delayed spectra obtained with high multiplicity ($\sim$ 8-9) condition. A rough estimate gives a lifetime of $\sim$ 5 ns and a possible spin of $\sim$ 17-19 $\hbar$. A candidate for this state could be a level of energy 7763 keV deexcited via a 178 keV γ-ray (not shown in Fig. 6).

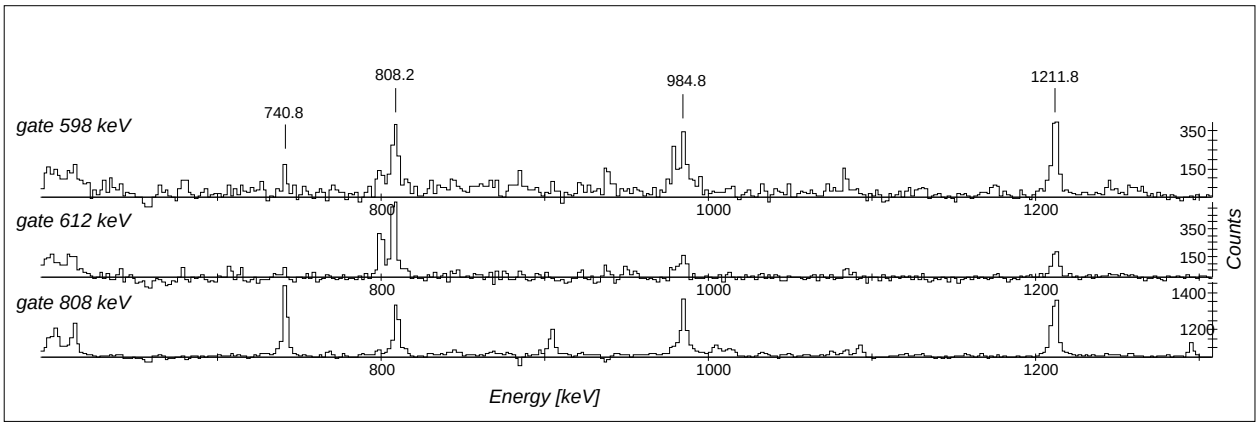

Figure 7: Examples of $\gamma\gamma$ coincidence spectra gated on the 598 and 612 keV transitions from the low spin part and by the 808 keV transition from the high spin part of the intruder band observed in the $^{98}Mo(^{16}O, 4n\gamma)$ reaction at 80 MeV bombarding energy.

3.1.5 The band-like structures 4 and 6 and upper part of band 5 (g.s. band).

A cascade of 312, 1250 and 275 keV transitions of M1+E2 character (with significant admixture of E2), labeled in Fig. 6 as band 4, is strongly connected to the g.s. band 5 via a 275 keV transition deexciting the 6^+, 2752 keV state. Based on the angular distributions and DCO results, one can propose (7^+) and (8^+) assignments for the 4002 and 4314 keV levels, respectively. However the 8^+ and 9^+ assignments cannot be completely ruled out. In the case of the 4314 keV level both assignments are in agreement with an E1 character for the 383 keV

Table 3: *Experimental B(E2), γ-ray branching ratios (λ) in light Sn isotopes. Subscripts i and y denote intraband and interband transitions (to the yrast or side bands), respectively. Intensities I_γ are given with reference to the 1212 keV (^{110}Sn), 979 keV (^{111}Sn) and 1257 keV (^{112}Sn) γ-rays, respectively.*

^{A}X	$E_x^{init.lev.}$ (keV)	E_γ (keV)	I_i	I_f	I_γ	$\lambda=\frac{i\to i}{i\to y}$	$K_{exp}=\frac{B(E2)_{intraband}}{B(E2)_{interband}}$
^{110}Sn	3215	368	$(4^+)_i$	$(2^+)_i$	0.10±0.03	≤5	$\geq 1.7*10^4$
		2014	$(4^+)_i$	$(2^+)_y$	≤0.02		
	3215	368	$(4^+)_i$	$(2^+)_i$	0.10±0.03	0.14±0.08	5.6±3.1
		760	$(4^+)_i$	$(6^+)_y$	0.70±0.3		
	3813	598	$(6^+)_i$	$(4^+)_i$	3.5 ±0.21	≤50	≥4545
		1626	$(6^+)_i$	$(4^+)_y$	≤0.1		
	4425	612	$(8^+)_i$	$(6^+)_i$	2.6±0.03	≤20	≥4745
		1955	$(8^+)_i$	$(6^+)_y$	≤0.05		
	5227	802	$(10^+)_i$	$(8^+)_i$	2.80±0.10	8.3±1.6	15.6±2.2
		913	$(10^+)_i$	$(8^+)_y$	0.30±0.10		
	6035	808	$(12^+)_i$	$(10^+)_i$	9.80±0.70	25±8	79±25
		1019	$(12^+)_i$	$(10^+)_y$	0.44±0.13		
	6035	808	$(12^+)_i$	$(10^+)_i$	9.80±0.70	12±2	12±2
		817	$(12^+)_i$	$(10^+)_y$	0.80±0.10		
^{111}Sn	4074	768	$(23/2^-)_i$	$(19/2^-)_i$	13.60±0.70	1.1±0.1	6.3±0.5
		1091	$(23/2^-)_i$	$(19/2^-)_y$	12.40±0.80		
	4074	768	$(23/2^-)_i$	$(19/2^-)_i$	13.60±0.70	2.2±0.2	6.4±0.6
		951	$(23/2^-)_i$	$(19/2^-)_y$	6.20±0.50		
	4074	768	$(23/2^-)_i$	$(19/2^-)_i$	13.60±0.70	2.7±0.1	4.3±0.2
		846	$(23/2^-)_i$	$(19/2^-)_y$	5.10±0.07		
	4074	1091	$(23/2^-)_i$	$(19/2^-)_i$	12.40±0.80	2.0±0.2	1.1±0.1
		951	$(23/2^-)_i$	$(19/2^-)_y$	6.20±0.50		
	5746	869	$(31/2^-)_i$	$(27/2^-)_i$	21.00±1.00	4.7±0.4	5.8±0.5
		907	$(31/2^-)_i$	$(27/2^-)_y$	4.55±0.05		
	3620	637	$(23/2^-)_i$	$(19/2^-)_i$	5.00±0.50	50±20	1.5±0.8
		314	$(23/2^-)_i$	$(19/2^-)_y$	0.10±0.20		
^{112}Sn	3416	893	$(6^+)_i$	$(4^+)_i$	1.43±0.50	0.4±0.2	1.7±0.7
		1167	$(6^+)_i$	$(4^+)_y$	3.30±0.82		
	3416	631	$(6^+)_i$	$(4^+)_i$	2.05±0.64	0.6±0.3	13.4±5.3
		1167	$(6^+)_i$	$(4^+)_y$	3.30±0.82		
	5568	745	$(12^+)_i$	$(10^+)_i$	2.86±0.62	7.8±3.7	19±10
		888	$(12^+)_i$	$(10^+)_y$	0.36±0.25		
	6367	800	$(14^+)_i$	$(12^+)_i$	5.19±0.81	5.3±2.5	2.4±1.4
		680	$(14^+)_i$	$(12^+)_y$	0.98±0.25		

transition linking this level with the 9^-, 3931 keV state from band 1. A second cascade, feeding the 6^+ yrast state found in this work consists of the 1227, 1191 and 323 keV transitions (band 6) starting from the 5218 keV level. The connection of this level with the (12^+), 6035 keV state of the intruder band via a weak 817 keV transition suggests a high spin for this state. A similar structure consisting of 1204 and 1335 keV transitions is placed at the top of 6_1^+ yrast state (band 5). Also in this case a weak connection (1019 keV) between the 6035 keV and 5016 keV levels is observed pointing for a high spin assignment for the latter level. The 1204, 1335 as well as 1227 and 1191 keV transitions having most likely a stretched E2 character, might suggest that the 5218 and 5016 keV levels are the missing 10^+ states, we are searching for.

3.1.6 Band 7

The 2058, 2455, 2742, 2821 and 3210 keV levels are introduced relaying on coincidence relations with the 985 and 1212 keV γ rays from the g.s. band. The level order and possible spin assignments are based on intensity and coincidence relations as well as on life-time information giving the recommended upper limits for γ-ray strengths [15].

3.1.7 Band 8

A spectrum gated on the 843 keV transition, which has most probably E2 character shows a previously unreported sequence of 817, 743, 850, 868 and 943 keV transitions. Based on the regular character of this cascade resembling the behavior of stretched quadrupole transitions in a rotational-like band, tentative spins up to $14\hbar$ are proposed. Information concerning the multipolarities of these transitions is strongly obscured because each of the considered peaks is placed on the tail of a stronger transition.

3.2 The nucleus ^{111}Sn

The level scheme of ^{111}Sn is presented in Fig. 8 and the γ-rays assigned to this nucleus are listed in Table 4. Fig. 9 displays a γ-ray spectrum gated on the 921 keV transition showing γ-rays from the g.s. band and from the two side bands, while spectra gated on the 942 and 1245 keV transitions are demonstrating the higher spin part of the intruder band. The present investigation confirms, with few a exceptions, the levels previously found [6, 7, 8, 9].

Table 4: *Gamma-ray transitions assigned to ^{111}Sn. Excitation energies of the initial state (E_i), γ-ray energies E_γ, relative intensities I_γ, angular correlation ratios R_{DCO} and angular distribution coefficients $W(\theta)$ as well as proposed spin and parity assignments are given.*

E_i (keV)	E_γ (keV)	I_γ (relative)	R_{DCO}	$W(\theta)$ A_2/A_0	A_4/A_0	$J_i^\pi \rightarrow J_f^\pi$ ($\hbar$)
979	978.5(0.1)	100(8)	1.04(10)	0.23(7)	-0.07(4)	$11/2^- \rightarrow 7/2^+$
1349	370.0(0.2)	$\leq$0.3				$11/2^- \rightarrow 11/2^-$
1349	1348.6(0.2)	23(9)	—	0.36(12)	0.06(17)	$11/2^+ \rightarrow 7/2^+$
2062	1083.4(0.1)	91(4)	0.71(23)	0.11(2)	-0.07(3)	$15/2^- \rightarrow 11/2^-$
2065	716.4(0.2)	5.0(9)	—	0.48(19)	0.04(11)	$15/2^+ \rightarrow 11/2^+$

2257	191.9(0.2)	1.6(2)	—	—	—	$19/2^+ \rightarrow 15/2^+$
2983	726.0(0.6)	0.4(2)	—	—	—	$19/2^- \rightarrow 17/2^+$
2983	921.2(0.1)	40(2)	1.54(25)	0.31(8)	-0.06(17)	$19/2^- \rightarrow 15/2^-$
3124	866.5(0.4)	1.2(2)	—	—	—	$19/2^- \rightarrow 17/2^+$
3124	1061.5(0.1)	21(1)	1.05(27)	0.39(9)	-0.02(2)	$19/2^- \rightarrow 15/2^-$
3228	1165.8(0.1)	8(1)	—	0.02(4)	-0.18(10)	$19/2^- \rightarrow 15/2^-$
3307	1244.7(0.1)	18(1)	0.73(29)	0.29(9)	-0.10(1)	$19/2^- \rightarrow 15/2^-$
3323	198.7(0.1)	6.2(3)	0.51(13)	0.07(13)	0.01(1)	$21/2^- \rightarrow 19/2^-$
3323	339.6(0.1)	6.5(4)	1.00(17)	-0.16(12)	0.18(43)	$21/2^- \rightarrow 19/2^-$
3459	475.9(0.1)	5.7(6)	0.90(30)	0.22(14)	-0.10(9)	$23/2^- \rightarrow 19/2^-$
3620	297.4(0.1)	2.2(2)	2.33(61)	0.25(17)	0.17(41)	$23/2^- \rightarrow 21/2^-$
3620	313.9(0.3)	0.1(2)	—	—	—	$23/2^- \rightarrow 19/2^-$
3620	636.7(0.1)	5.0(5)	—	—	—	$23/2^- \rightarrow 19/2^-$
3788	465.1(0.1)	5.5(4)	1.01(22)	0.38(14)	-0.02(6)	$25/2^- \rightarrow 21/2^-$
3956	971.8(0.1)	8.3(8)	—	—	—	$(23/2) \rightarrow 19/2^-$
4074	751.6(0.7)	1.0(3)	—	—	—	$23/2^- \rightarrow 21/2^-$
4074	767.9(0.1)	13(1)	0.62(25)	0.33(11)	-0.05(4)	$23/2^- \rightarrow 19/2^-$
4074	845.8(0.2)	5.1(5)	—	—	—	$23/2^- \rightarrow 19/2^-$
4074	950.8(0.2)	6.2(5)	—	—	—	$23/2^- \rightarrow 19/2^-$
4074	1090.8(0.1)	12 (1)	—	—	—	$23/2^- \rightarrow 19/2^-$
4155	367.1(0.2)	2.0(2)	0.86(19)	—	—	$25/2^- \rightarrow 25/2^-$
4446	1123.3(0.2)	3.6(4)	1.87(75)	—	—	$25/2^- \rightarrow 21/2^-$
4839	1218.5(0.2)	6.0(6)	—	0.004(4)	-0.18(8)	$27/2^- \rightarrow 23/2^-$
4877	802.9(0.1)	27 (1)	0.85(12)	0.32(93)	-0.05(3)	$27/2^- \rightarrow 23/2^-$
4877	1088.6(0.5)	1.5(3)	—	—	—	$27/2^- \rightarrow 25/2^-$
4988	914.6(0.2)	5.2(6)	—	—	—	$(27/2) \rightarrow 23/2^-$
4988	1033.1(0.2)	5.6(6)	—	—	—	$(27/2) \rightarrow (23/2)$
5746	869.4(0.1)	21(1)	1.08(21)	0.25(10)	-0.08(23)	$31/2^- \rightarrow 27/2^-$
5746	907.1(0.2)	4.5(3)	—	—	—	$31/2^- \rightarrow 27/2^-$
5767	889.8(0.2)	3.4(4)	—	—	—	$(29/2^-) \rightarrow 27/2^-$
5767	927.4(0.3)	2.7(3)	—	—	—	$(29/2^-) \rightarrow 27/2^-$
6130	364.8(0.9)	0.6(3)	—	—	—	$(31/2) \rightarrow (29/2^-)$
6130	1141.7(0.5)	2.0(5)	—	—	—	$(31/2) \rightarrow (27/2)$
6130	1254.1(0.3)	3.3(5)	—	—	—	$(31/2) \rightarrow 27/2^-$
6689	942.4(0.7)	20(1)	0.75(17)	0.10(11)	-0.13(12)	$35/2^- \rightarrow 31/2^-$
6843	1076.0(0.1)	7.7(6)	—	—	—	$(31/2^-) \rightarrow (29/2^-)$
6843	1096.7(0.2)	6.1(7)	—	—	—	$(31/2^-) \rightarrow 31/2^-$
7684	995.3(0.9)	12(7)	—	0.30(18)	-0.05(6)	$(39/2^-) \rightarrow 35/2^-$
8739	1054.6(0.1)	7.4(5)	—	—	—	$(43/2^-) \rightarrow (39/2^-)$
9861	1121.8(0.2)	3.2(3)	—	—	—	$(47/2^-) \rightarrow (43/2^-)$
11082	1221.3(0.3)	2.1(3)	—	—	—	$(51/2^-) \rightarrow (47/2^-)$

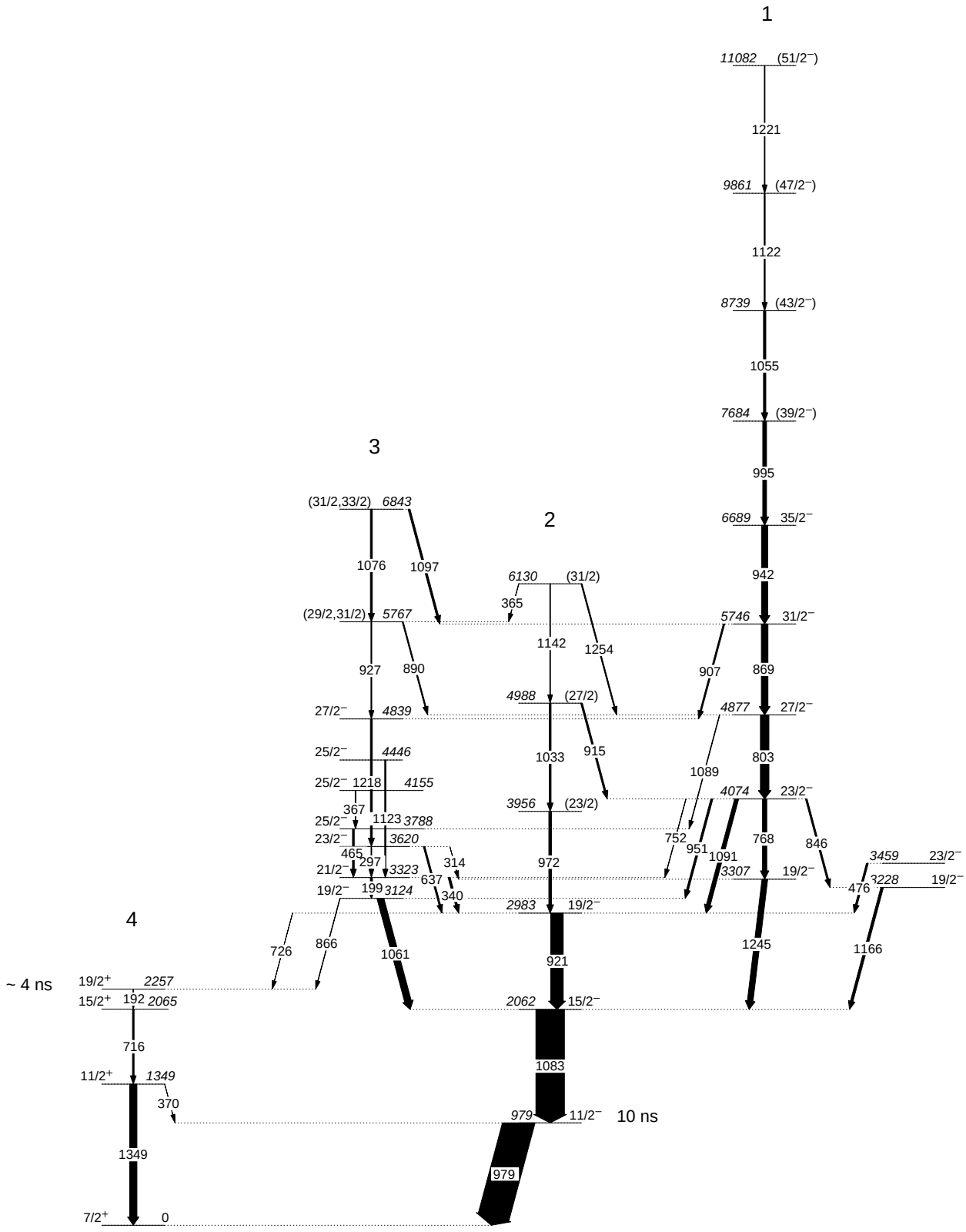

Figure 8: Level scheme of ^{111}Sn obtained in the $^{98}Mo(^{16}O, 3n)$ reaction.

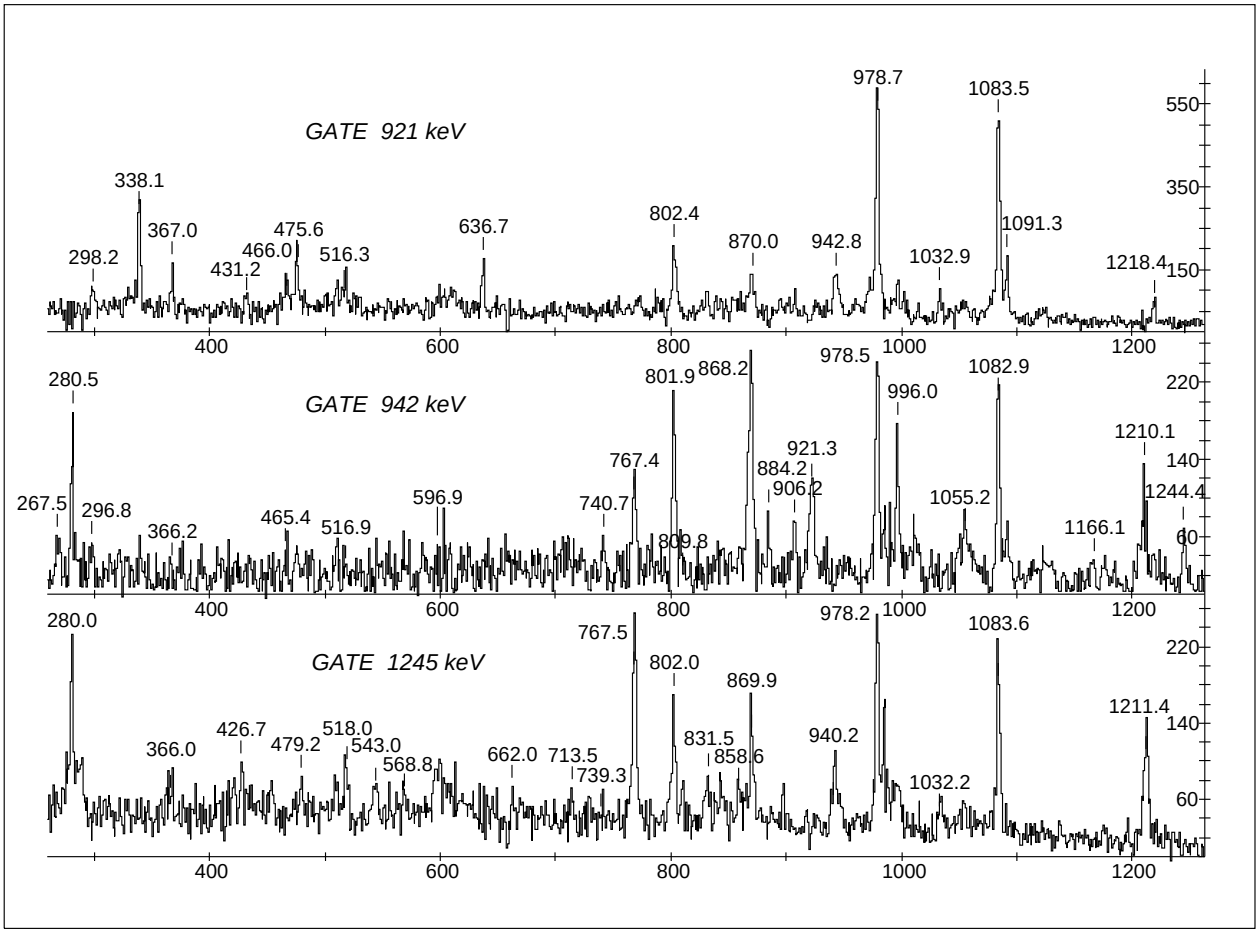

Figure 9: High energy parts of the background corrected, coincident spectra obtained for ^{111}Sn in the 3n reaction. Spectra gated by 942 and 1245 keV transitions demonstrate higher spin part of the intruder band, while spectrum gated on 921 keV line shows lines from bands 1, 2 and 3.

3.2.1 Band 1

An intruder band built on the $23/2^-$, 4074 keV level being connected by stretched quadrupole transitions has been established in previous studies [6, 17]. In the present work it was found that the decay of the 4074 keV level, is very fragmented. Apart from the relatively strong 768 and 1091 keV γ-rays, it decays also through weaker 752, 846 and 951 keV transitions. Four $19/2^-$ states are populated in this decay. Branching ratios of the intra- to inter-band E2 transitions for the 4074 and 5746 keV levels are given in Table 3.

3.2.2 Band 2

The g.s. band, previously known up to the $19/2^-$, 2983 keV level [6, 17] was extended up to a tentatively introduced $(31/2^-)$, 6130 keV level deexciting via a sequence of weak 1142, 1033 and 972 keV transitions feeding the 2983 keV level.

3.2.3 Band 3

A second negative parity sequence (band 3) was known previously [7] up to the $27/2^-$, 4839 keV level. An extension to the $(31/2^-, 33/2^-)$, 6843 keV level is proposed.

3.2.4 Band 4

A cascade of 192(M1+E2)-716(E2)-1349(E2) keV transitions (Figs. 8 and 10), feeding directly the $7/2^+$ ground state and forming the only positive parity sequence in ^{111}Sn has been found in the coincidence spectra shown in Fig. 9. In addition to the known [6] isomeric state at 979 keV an indication has been found for a new isomer in ^{111}Sn with a half life of $T_{1/2} \sim 4$ ns at an excitation energy of 2257 keV. A spin $17/2^+$ or $19/2^+$ is proposed for this isomer. The above mentioned cascade is rather weak and only a limit for the life-time of the 2257 keV level could be established. By a comparison with the known (remeasured in the present work) isomeric state at 979 keV with the half-life of about 10 ns one can conclude that the life-time of the 2257 keV level should be shorter than 10 ns and longer or equal to 4 ns (see subsection 5).

3.3 Other nuclei populated in the $^{98}Mo(^{16}O, xnyp)$ reaction

In the present experiment, with the $^{98}Mo(^{16}O, xnyp)$ reaction, and $^{114}Sn^*$ as a compound nucleus, γ-ray transitions belonging to 15 residual nuclei (Table 1) are identified. Among those the $19/2^+$, 210 ms isomeric state and its deexcitation is observed in the nucleus ^{109}In (p4n reaction channel). Moreover, in the odd-odd nucleus ^{110}In doublet bands which could be interpreted as a manifestation of chirality in the angular momentum coupling are observed however, they still need further investigation.
The intruder band reported [17] in nucleus ^{111}In (p2n reaction channel) is not confirmed in the present experiment with the $E_{^{16}O}$=80 MeV beam energy, even in its low-spin part.
Between the beam bursts (3-4.5 ms) mainly the radioactive decay to ^{110}In, populating levels up to the 9^+, 3191 keV level from the g.s. band and up to 7^-, 3125 keV and 6^+, 3068 keV in the side bands in ^{110}Cd is observed. The lowest levels in ^{111}Cd, the daughter nucleus of ^{111}In, are also observed showing a new connection (via a 220 keV transition) with the $11/2^-$, 48 min. isomeric state. For ^{112}Sn the branching ratios of the enhanced intra-band E2 to the unfavoured

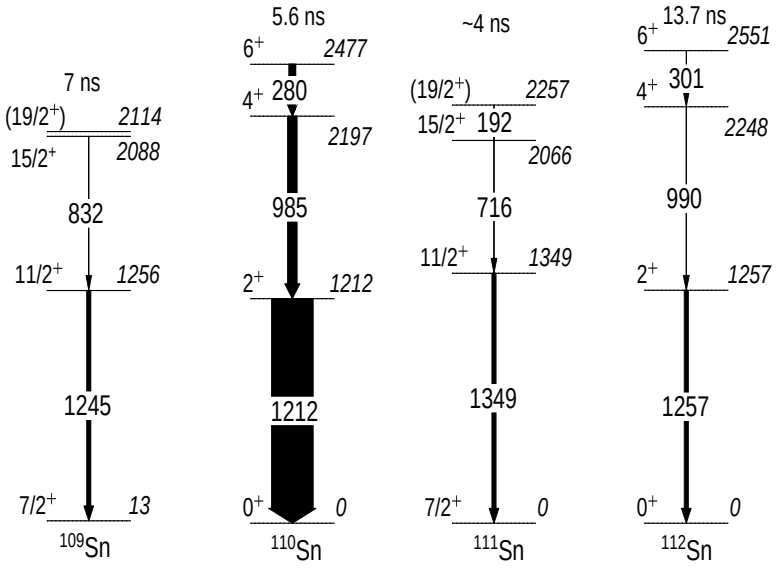

Figure 10: The $g_{7/2}$ neutron-core coupling in ^{111}Sn and the lowest excited states in the neighboring nuclei ^{109}Sn, ^{110}Sn and ^{112}Sn (see disscusion in subsection 4.3).

inter-band transitions with the same multipolarity have been obtained and are listed in Table 3.

4 Discussion

4.1 Positive parity states in ^{110}Sn

A systematics of the positive parity states in light even-A Sn nuclei is presented in Fig. 11. The energies of the yrast states in these nuclei increase with increasing neutron number up to ^{112}Sn and then start to decrease. In contrast, the energies of the second 10^+ and the 12^+ states show a permanent decrease with a increasing neutron number. The (8^+), 3812 keV and (10^+), 5016 keV yrast states established in ^{110}Sn in this work and the 10^+, 5227 keV and (12^+), 6035 keV levels from the intruder band found in earlier studies nicely fit into this systematics. In each of even Sn isotopes above ^{106}Sn, at least two 10^+ excited states have been observed [16]. They are interpreted as 2particle-2hole: $\pi g_{7/2} d_{5/2} g_{9/2}^{-2}$ and 2-particle: $\nu h_{11/2}^2$ states. The systematics of 10^+ states shown in Fig. 11 implicate a suggestion that these states may change their character in the nucleus ^{110}Sn.

The experimental branching ratios $\frac{B(E2)_{intr}}{B(E2)_{inter}}$ for the intruder band in ^{110}Sn, given in Table 3, show that in the high-spin region intra-band E2 transitions are very strong as compared to the the hindered inter-band transitions of the same multipolarity, while in the low-spin region the intensities of these transitions are comparable. This indicates that the low-spin states are mixed (perturbed) contrary to the high-spin states with pure configurations. In the align-

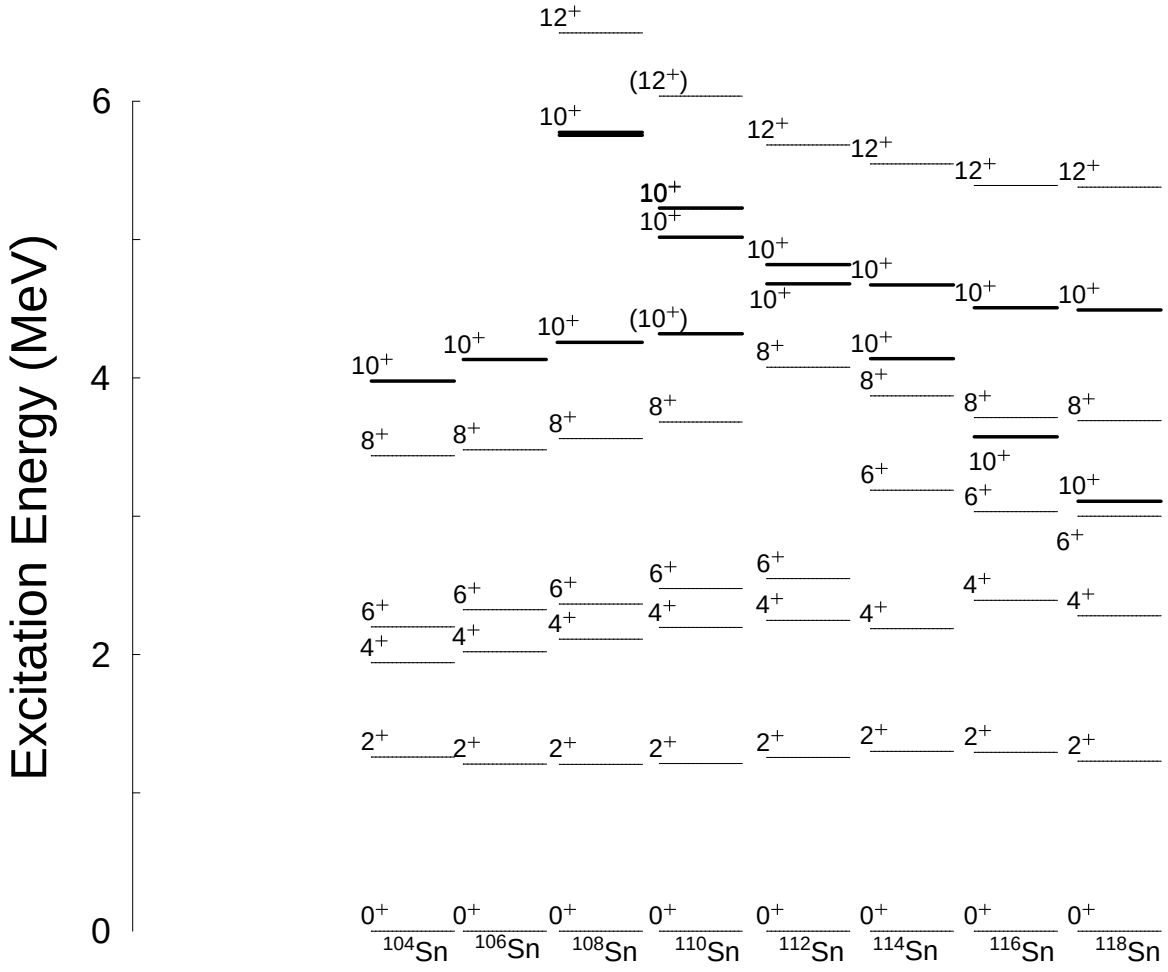

Figure 11: Systematics of the positive-parity states in even-A Sn isotopes

ment plot (Fig. 12), this mixing manifests itself as an irregularity at low rotational frequencies .

The alignment plots for ^{110}Sn and ^{112}Sn look similar in many aspects. The band crossing in the intruder band occurs at $\hbar\omega \approx 0.37$ MeV in ^{110}Sn and ≈ 0.35 MeV in ^{112}Sn while the increase in the alignment is about $7\hbar$ for both of them. In this mass region the first band crossing has usually been attributed to the $h_{11/2}$ neutrons [10, 19]. The intra-band B(E2) values in the intruder bands of ^{112,114,116,118}Sn were also analyzed within the framework of the IBM1 model [20]. A detailed comparison of these bands with the ground state bands in the even-mass Xe isotopes allows [20] to find a similarity in the energy spacings as well as in the B(E2) values. In the introduction, it was pointed out that the structure of the low-lying states in Sn is dominated by neutron excitations. Configuration assignments in ^{110}Sn can be achieved by comparison with the shell model configurations assigned to the nuclei ^{106}Sn and ^{108}Sn [16]. As the $\nu(d_{5/2}g_{7/2})$ configuration is already assigned to the 6^+, 2477 keV level, the second 6^+ state

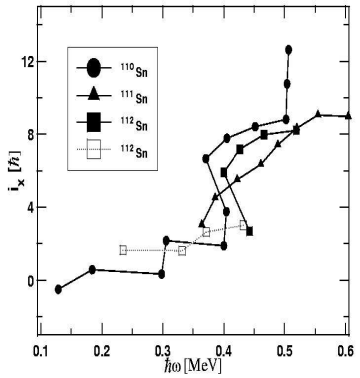

Figure 12: Experimental alignments for the intruder bands in the ^{110}Sn, ^{111}Sn and ^{112}Sn nuclei. A reference configuration with parameters $J_0 = 15\hbar^2\ MeV^{-1}$ and $J_1 = 25\hbar^4\ MeV^{-3}$ has been subtracted. An upbend at $\hbar\omega \sim 0.5$ MeV may suggests a significant change in nuclear structure of ^{110}Sn.

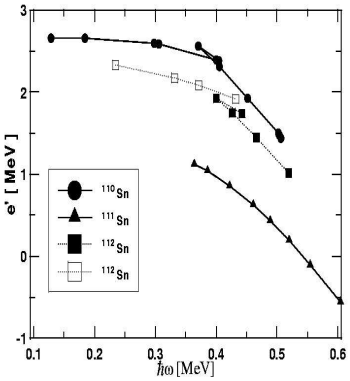

Figure 13: Experimental routhians for intruder bands in the nuclei ^{110}Sn, ^{111}Sn and ^{112}Sn. A reference configuration with parameters $J_0 = 15\hbar^2\ MeV^{-1}$ and $J_1 = 25\hbar^4\ MeV^{-3}$ has been subtracted. The crossing frequency in ^{110}Sn and ^{112}Sn is found around 0.37 MeV, while in ^{111}Sn the first $\nu h_{11/2}$ alignment is shifted due to the occupation of the $\nu h_{11/2}$ orbital.

at 2752 keV may originate from the $\nu g^2_{7/2}$ configuration while to the third 6^+ state at 2800 keV the $\nu(d^2_{5/2}g^2_{7/2})$ or $\nu(d_{5/2}g^3_{7/2})$ configurations can be proposed.
At higher spins, level patterns similar to the $6^+ \rightarrow 4^+ \rightarrow 2^+ \rightarrow 0^+$ yrast sequence appear in the level scheme of ^{110}Sn indicating that certain states can be interpreted as two- or four-quasi-particle excitations coupled to collective low-lying states. The level sequences built on the two last-mentioned 6^+ states (band 4 and band 6) are consistent with such a description. The observed pattern can be compared with the low-lying level structures in ^{110}Cd, ^{111}In and ^{112}Sn.

4.2 Negative parity states in ^{110}Sn

Negative parity two-quasiparticle states involve one neutron occupying the $h_{11/2}$ orbital. The 2458, 2963 (or 3354), 3686 and 3931 keV levels (see Fig. 14 and band 1 in Fig. 6) are proposed to be the 3^-, 5^-, 7^- and 9^- members of the $\nu(g_{7/2}h_{11/2})$ multiplet with a small admixture of the $\nu(d_{5/2}h_{11/2})$ and/or $\nu(d_{3/2}h_{11/2})$ configurations. The energy spacings between the 9^- and 11^- as well as 11^- and 13^- states are very close to the energy of the 2^+ state in ^{108}Sn. Thus the 5106 and 6544 keV states may originate from the fully aligned $\nu(g_{7/2}h_{11/2})_{9^-}$ member of the multiplet coupled to the 2^+ and 4^+ states in ^{108}Sn, respectively. Their experimental energies are quite correctly reproduced in the zero-order approximation, i.e. by summing of the corresponding level energies. The fact that both states decay via E2 transitions further supports the proposed interpretation. Shell model calculations [21] performed assuming ^{100}Sn as a closed core and

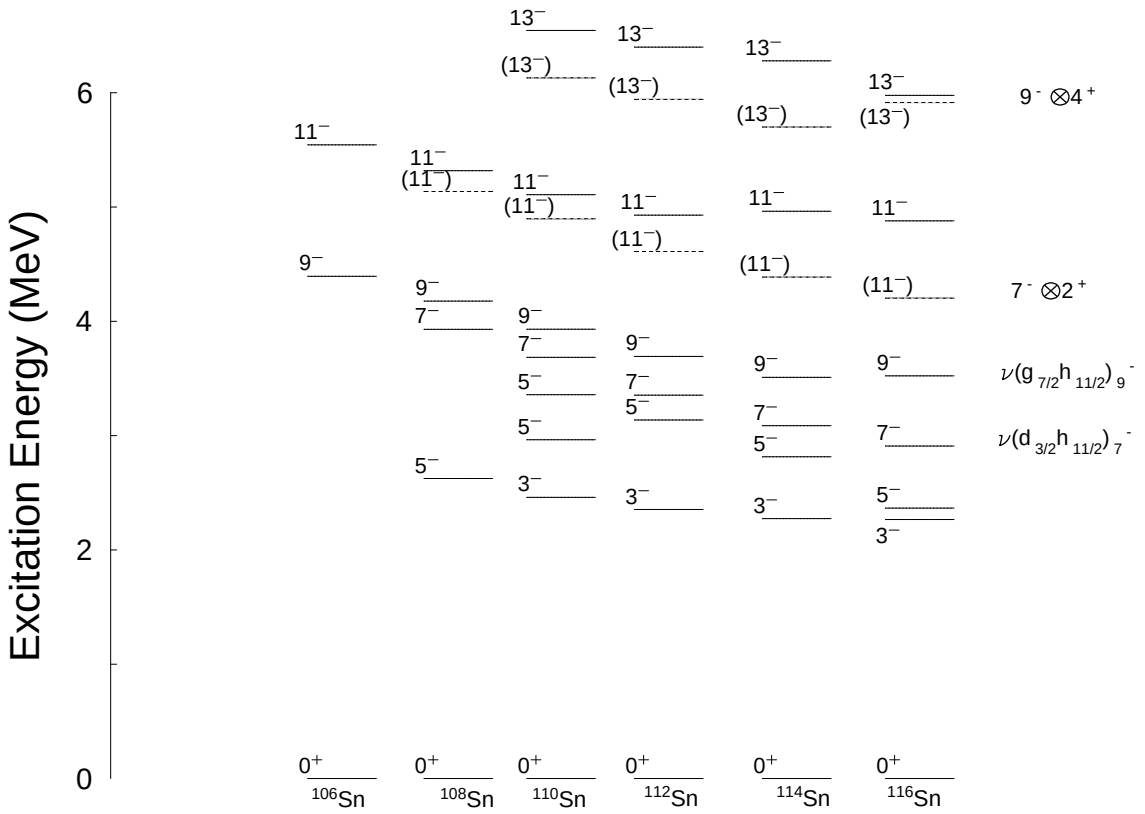

Figure 14: Systematics of negative parity states in selected even-A Sn isotopes

10 valence neutrons occupying five single-particle orbits in the 50-82 shell nicely reproduce the energies of the negative parity states in ^{110}Sn.

4.3 Excited states in the nucleus ^{111}Sn

An extention of the g.s. band above the $19/2^-$, 2983 keV state is weakly developed and there is still an open question of the spin-parity assignments for the 3956, 4988 and 6130 keV levels which may have positive parities as observed in ^{115}Sn [23]. In such case these states could arise from the $h^2_{11/2}g_{7/2}$ multiplet.

The deformed intruder band in ^{111}Sn which was proposed [6] to originate from the $\nu h_{11/2}$ orbital coupled to the deformed proton 2p2h excitation across the Z=50 shell gap, is also observed in the present experiment. The configuration proposed for this structure is $\nu h_{11/2} \otimes [(\pi g_{7/2})^2 (\pi g_{9/2})^{-2}]$ [6] or $\nu h_{11/2} \otimes [\pi (g_{7/2} d_{5/2})^2 g_{9/2})^{-2}]$ [22]. This band develops on top of the $23/2^-$ state origin-

ating from the $\nu h_{11/2} \otimes 6^+$ configuration . It decays to at least four $19/2^-$ states arising from couplings of the $h_{11/2}$ neutron to the spherical and deformed 4^+ and 6^+ states in ^{110}Sn.
The negative parity band 3 may originate from the $h_{11/2}$ orbital coupled to the 4^+, 6^+, 8^+ and 10^+ states in ^{110}Sn. The 3124 keV state can be interpreted as a fully aligned member of the $\nu h_{11/2} \otimes 4^+$ multiplet. The maximum spin state from the $\nu h_{11/2} \otimes 10^+$ configuration is 31/2 which may be assigned to the 6843 keV state.

The nature of the 2257 keV, possibly an isomeric state, may be explained if one assumes that the observed levels in ^{111}Sn result from the coupling of the $g_{7/2}$ neutron to the closed neutron shell excitations of the $^{110}_{50}Sn_{60}$ core (Fig. 10). Therefore, one can expect that the 192 keV transition in ^{111}Sn should be of the same nature as the 280 keV transition between the 6_1^+ and 4_1^+ states in ^{110}Sn, i.e. it should be of hindered E2 character. Since the $g_{7/2}$ neutron is a spectator, the reduced transition probability $B(E2; 19/2^+ \rightarrow 15/2^+)$ is proportional to $B(E2; 6^+ \rightarrow 4^+)$. Therefore the life-time of the 2257 keV, $19/2^+$ state in ^{111}Sn can be deduced from the half-life of the 6^+ state in ^{110}Sn by taking only into account the energy dependence of $T_{1/2}$. The 6^+ state in ^{110}Sn has a life-time of 5.6 ns [3], which gives for the 2257 keV level in ^{111}Sn a life-time of 37 ns, which is approximately an order of magnitude larger than the experimental value. This enhancement of the 192 keV transition ($B(E2; (19/2)^+ \rightarrow 15/2^+) = 263 e^2fm^2$) in comparison with the 280 keV transition ($B(E2; 6^+ \rightarrow 4^+) = 29 e^2fm^2$) can possibly be explained by the polarization effect. The neutron coupled to the excited core can polarize the latter and influence the effective charge, e_{eff}, what could result in an increase of the E2 transition probability.

4.4 TRS calculations and comparison with experimental data

In order to gain a better understanding of the band structure observed in experiment, self-consistent Total-Routhian-Surface (SC-TRS) calculations have been performed. The total Routhian was minimised on a lattice in the (β_2, γ) space with hexadecapole deformation β_4 included in the calculation. The deformed Woods-Saxon potential with a new set of parameters adapted and incorporated into the TRS program by R. Wyss was used as a single-particle potential. For a detailed description of this model see Refs. [24, 25] and references quoted therein. Examples of TR surfaces for the yrast configuration in ^{110}Sn are shown in Fig. 15.

The results of the calculations suggest a quadrupole deformation with the deformation parameters $\beta_2 \approx 0.2$ and $\gamma \approx$ -5° for the yrast band at rotational frequencies $\hbar\omega \leq 0.35$ ($I_x < 14\ \hbar$). However, the experimental data suggest that the levels in this region of excitation energies have not a pure rotational nature. Above the alignment of the $h_{11/2}^2$ neutrons at $\hbar\omega > 0.35$ MeV, the TRS calculations predict that the shape of nucleus becomes triaxial (with $\gamma \approx 15°$), but that the deformation parameter β_2 does not change. The 2-quasi-neutron $h_{11/2}^2$ configuration drives the nucleus towards a positive γ deformation, so, one can conclude that the angular momentum alignment (due to aligned neutrons) will influence significantly the evolution of the shape.
The calculated angular momenta and excitation energies are compared with the experimental data in Figs. 16 and 17, respectively.

One observes a satisfactory good agreement between calculated and experimental data until $\hbar\omega$=0.5, where distinct discrepancies appear. However, the plot of the total energy as function of angular momentum Fig. 17 does not exhibit such a discrepancy.

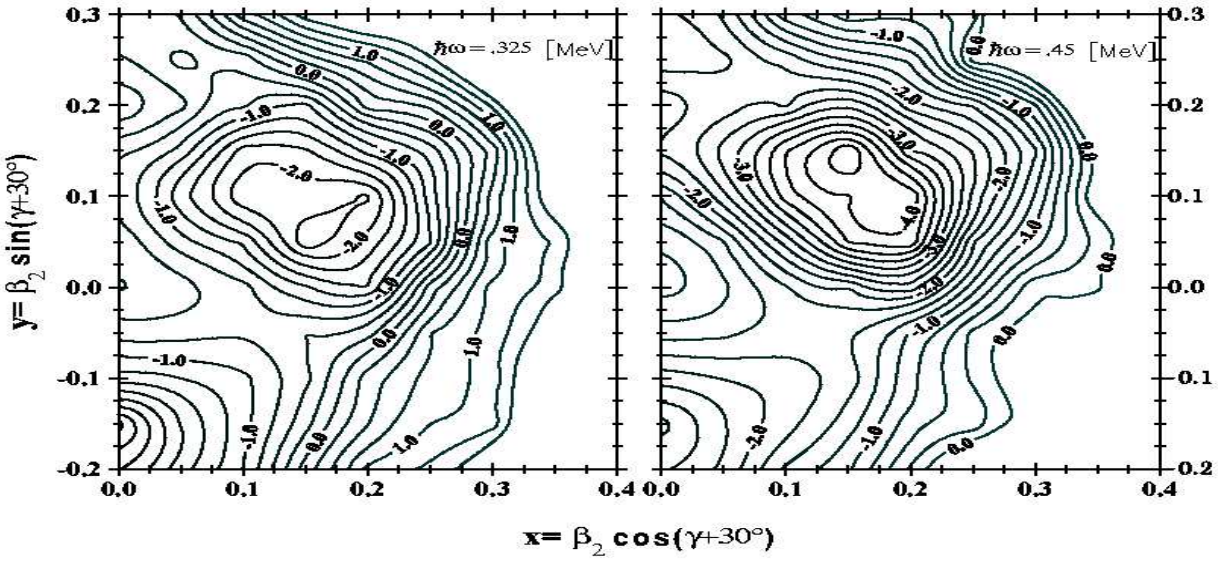

Figure 15: Total Routhian surfaces calculated for ^{110}Sn at the frequencies $\hbar\omega = 0.325$ MeV and $\hbar\omega = 0.45$ MeV, i.e. before and after neutron alignment, respectively. The distances between the contour lines is 250 keV.

In the case of ^{111}Sn, the calculations predict a prolate shape of the nucleus with a quadrupole deformation β_2 between 0.18 and 0.2 and γ between -2.3^o and -5^o.

5 Summary

Excited states in ^{110}Sn, ^{111}Sn and in neighboring nuclei have been investigated in the ^{98}Mo + ^{16}O reaction using the OSIRIS-II Ge detector array equipped with the multiplicity filter.
The results are:

- The main branches feeding the 6^+ isomer and the ground state cascade in ^{110}Sn are established based on coincidence relations, angular distribution measurements and relative excitation function data.
- The new band structures 2, 4, 6 and 7 are introduced into the level scheme of ^{110}Sn.
- The intruder band in ^{110}Sn (band 3) based on the deformed 2h-2p configuration is extended to the low-spin region.
- It is assumed that bands 1, 4, 5, 6, 7 and 8 in ^{110}Sn consist of spherical states built on neutron excitations forming a number of coexisting structures close to that of yrast band

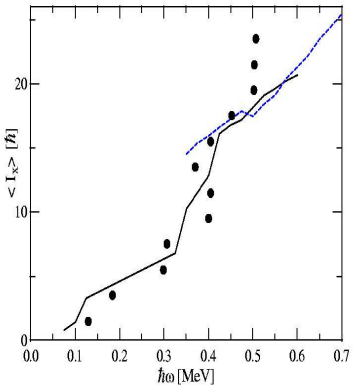

Figure 16: The calculated (solid $\gamma < 0$ and dashed $\gamma > 0$ lines) and experimental (dots) values of the total angular momentum as a function of rotational frequency in ^{110}Sn.

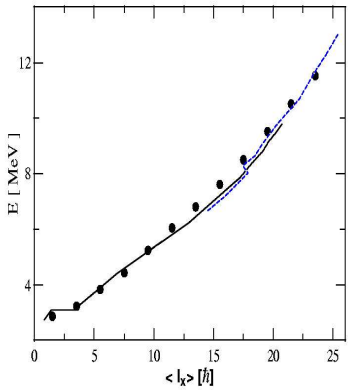

Figure 17: The calculated (solid $\gamma < 0$ and dashed $\gamma > 0$ lines) and experimental (dots) excitation energies as a function of total angular momentum in ^{110}Sn.

in ^{110}Sn. Band 4 is displying a pattern which obviously cannot be described within the deformed rotor picture.

- The newly proposed band 2 in ^{110}Sn most probably consists of a sequence of ΔI=1 transitions.
- It is assumed that the newly established cascade of $(19/2)^+ \rightarrow 15/2^+ \rightarrow 11/2^+ \rightarrow 7/2^+$ transitions results from a $g_{7/2}$ neutron coupled to the ^{110}Sn core.
- The intruder band in ^{111}Sn is confirmed and the g.s.band and the negative parity band is extended.
- The experimental B(E2) γ-ray branching ratios between the intruder and yrast states in the nuclei ^{110}Sn, ^{111}Sn and ^{112}Sn show rather strong intra-band B(E2) values compared to the hindered inter-band decays.
- An intruder band reported in ^{111}In [17] is not confirmed in the present experiment, even in its low-spin part.

6 Acknowledgements

We are very grateful to the staff of the Heavy Ion Laboratory at the Warsaw University for providing excellent beam conditions and for all support at each stage of the work. The work was financially supported by the Polish Committee for Scientific Research (grants KBN No. 2 P03B-02308 and No.5 P03B 03620).

References

[1] M. Singh, J.W. Sunier, R.M. Devries, G.E. Thompson, Nucl. Phys., **A193**, (1972), 449.

[2] D.A. Viggars, H.v. Taylor, B. Singh, J.C. Vaddington, Phys. Rev., **C36**, (1987), 1006.

[3] J. Bron, W.H.A. Hesselink, A.van Poelgeest, A.J.J. Zalmstra, J.M. Uitzinger and H. Verheul, Nucl. Phys., **A318**, (1979), 335.

[4] F. Azaiez, S. Andriamonje, J.F. Chemin, M. Fidah, J.N. Scheurer, M.M. Alèonard, G. Bastin, J.P. Thibaud, F. Beck, G. Costa, J.F. Bruandet, and F. Litard, Nucl. Phys., **A501**, (1989), 401.

[5] R. Wadsworth, H.R. Andrews, R.M. Clark, D.B. Fossan, A. Galindo-Uribarri, J.R. Hughes, V.P. Janzen, D.R. LaFosse, S.M. Mullins, E.S. Paul, D.C. Radford, H. Schnare, P. Vaska, D. Ward, J.N. Wilson, and R. Wyss, Nucl. Phys., **A559**, (1993), 461.

[6] D.R. LaFosse, D.B. Fossan, J.R. Hughes, Y. Liang, P. Vaska, M.P. Waring, and J.-Y. Zhang, Phys. Rev. C, **vol.51, no.6**, (1995), R2876.

[7] V.P. Janzen, Phys. Scripta, **vol. T56**, (1995), 144.

[8] M.E.J. Wigmans, R.J. Heynis, P.M.A. van der Kam, H. Verheul, Phys. Rev., **C14**, (1976), 229.

[9] P.J. Blankert, H.P. Blok, J. Blok, Nucl. Phys. **A356**, (1981), 74.

[10] J.L. Wood, K. Heyde, W. Nazarewicz, M. Huyse, and P. Van Duppen, Phys. Repts., **215**, (1992), 101.

[11] P. Kowina, High spin states in ^{110}Sn, Msc. Thesis, 1999.

[12] M. Wolinska-Cichocka, B. Bekman, Ch. Droste, J. Dworski, W. Gast, J. Iwanicki, H. Jäger, M. Kisieliński, A. Kordyasz, M. Kowalczyk, J. Kownacki, R. Lieder, W. Męczyński, T. Morek, M. Palacz, J. Perkowski, E. Ruchowska, J. Srebrny, A. Stolarz, and J. Styczeń, Acta Phys. Pol. **B34**, (2003), 2305 and **B34**, (2003), 2309.

[13] D.C. Radford, Nucl. Instrum. Methods **A236**, (1995), 297

[14] G.M. Crawley, W. Benenson, G. Bertsch, S. Gales, D. Weber, B. Zwięgliński, Phys. Rev.C., **vol.23, no.2**, (1981), 589.

[15] P.M. Endt, Atomic Data and Nu. Data Tables, **26**, (1981) 47-91.

[16] S. Juutinen, E. Mäkelä, R. Julin, M. Piiparinen, S. Törmänen, A. Virtanen, E. Adamides, A. Ataç, J. Blomqvist, B. Cederwall, C. Fahlander, E. Ideguchi, A. Johnson, W. Karczmarczyk, J. Kownacki, S. Mitarai, L.-O. Norlin, J. Nyberg, R. Schubart, D.Seweryniak, G. Sletten, *Nucl. Phys.* **A617**, (1997), 74.

[17] G. Gangopadhyay, A.K. Singh, D.Banerjee, R. Bhattacharya, R.K. Bhownik, S. Muralithar, G. Rodriguez, R.P. Singh, A. Goswami, S. Bhattacharya, B. Dasmahapatra, S. Sen, Z. Phys., **A351**, (1995), 1.

[18] P.E. Cavangh, C.F. Coleman, A.G. Hardacre, G.A. Gard, J.F. Turner, Nucl. Phys., **A141**, (1970), 97.

[19] K. Heyde, J. De Beule, B. Decroix, C. De Coster and A.M. Oros, CERN-EP/ **98-181**, (1998), 1.

[20] A.D. Efimov, Yu.N. Lobach, A.A. Pasternak, V.V. Tryshyn, - to be published and A.A. Pasternak - private communication.

[21] A. Covello, A. Gargano, P. Guazzoni, L. Zetta, G. Graw and M. Jaskóła, World Scientific, Singapore, **2002, p. 327**.

[22] R. Wadsworth, C.W. Beusang, M. Cromaz, J. DeGraaf, T.E. Drake, D.B. Fossan, S. Flibotte, A. Galindo-Uribari, K. Hauschild, G.Hackman, J.R. Hughes, V.P. Janzen, D.R. LaFosse, S.M. Mullins, E.S. Paul, D.C Radford, H. Schnare, P. Vaska, D. Ward, J.N. Ward, J.N. Wilson, and I. Ragnarsson, *Phys.Rev.C* **vol.53, no.6**, (1996), 2763.

[23] A. Savelius, S. Juutinen, K. Helariutta, P. Jones, R. Julin, P. Jämsen, M. Muikku, M. Piiparinen, J. Suhonen, S. Törmänen, R. Wyss, P.T. Greenlees, P. Simecek, D. Cutoiu, *Nucl.Phys* **A637**, (1998), 491.

[24] W. Satu la and R. Wyss, **Phys. Scri. Vol. T56** (1995) 159.

[25] K. Starosta, Ch. Droste, T. Morek, J. Srebrny, D.B. Fossan, D.R. LaFosse, H. Schnare, I. Thorslund, P. Vaska, M.P. Waring, W. Satuła, S.G. Rohoziński, R. Wyss, I.M. Hilbert, R. Wadsworth, K. Hauschild, C.W. Beausang, S.A. Forbes, P.J. Nolan and E.S. Paul, **Phys. Rev. C53** (1996) 137.